Renewable Energy 237 (2024) 121577

Contents lists available at ScienceDirect

Renewable Energy

journal homepage: www.elsevier.com/locate/renene

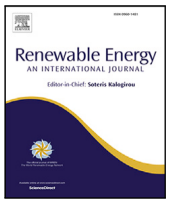

HAMS-MREL, a new open source multiple body solver for marine renewable energies: Model description, application and validation

Vaibhav Raghavan [a,*], Eva Loukogeorgaki [b], Nikos Mantadakis [b], Andrei V. Metrikine [a], George Lavidas [a]

[a] Delft University of Technology, Stevinweg 1, Delft, 2628 CN, Zuid Holland, Netherlands
[b] Aristotle University of Thessaloniki, Thessaloniki, 54124, Greece

ARTICLE INFO

Keywords:
Renewable energy
Multi-body interaction
BIEM
HAMS
HAMS-MREL
Validation
Open-source

ABSTRACT

With the rapid development of offshore renewable energy technologies, open source solvers for hydrodynamic analysis can become beneficial to meet the numerical challenges within the field, particularly when they are both accurate and computationally efficient. Hydrodynamic Analysis of Marine Structures (HAMS), a recently developed open source Boundary Integral Equation Method (BIEM) frequency domain solver has been shown to be a reliable, robust and computationally efficient for analysing single floating structures. This research enhances the capabilities of HAMS further by developing and incorporating a multiple body interaction formulation (henceforth referred as HAMS-MREL), which allows the solution of the diffraction and the radiation problem for multiple floating structures, taking into account their interaction. To evaluate proper performance of this new multi-body solver, comparisons are performed with semi-analytical solutions, as well as with the commercial solver WAMIT in terms of the hydrodynamic coefficients and exciting forces. The excellent comparison with semi-analytical solutions demonstrates the validity of the enhanced multi-body version of HAMS. In addition, the computational comparison considering lower order panels between HAMS-MREL and WAMIT (no symmetry) show that for deep water cases, HAMS-MREL is generally faster than WAMIT, while for the finite depth cases, it is slower. Finally, the functionality to utilize OpenMP parallelization within the multi-body formulation has been added, aiming to reduce the analysis time significantly for the finite depth cases, offering an expected improvement for the future.

1. Introduction

The global population has increased from 2.5 billion people in 1950 to over 8 billion at the end of 2022, wherein the last 3 billion people have been born since 1998. The world's population is expected to go to 9.7 billion in 2050 [1]. With the world's population growing rapidly, dependence on fossil fuels is no longer a viable option. Therefore, development of more renewable forms of energy particularly marine renewables has gained traction in the last two decades, and challenging energy targets have been set for the future. The strategy from the European Union has set targets to deploy 60 GW of offshore wind and 1 GW of wave energy by 2030, and 300 GW of offshore wind and 40 GW of wave energy by 2050 [2].

In order to achieve these set targets with low Levelised Cost of Energy (LCoE), wave energy converters (WECs) and floating offshore wind turbines (FOWT) need to be deployed in large numbers (farms). In addition to independent wave farms/offshore wind farms, collocated wind-wave systems and hybrid wind-wave systems will also be required since they offer many synergies including enhanced yield, smoothed power output, common grid infrastructure, shared operation and maintenance etc. [3].

Wave-structure hydrodynamic interactions considering multiple bodies play an important role when studying the behaviour of wave farms, collocated wind-wave systems and hybrid wind-wave systems. Therefore, detailed studies on this are important. Sismani et al. [4] studied the diffraction and scattering effects due to bottom fixed offshore wind turbine foundation on the wave field considering regular and irregular waves, and concluded that the fields depend heavily on the incident wave angle and peak period. Furthermore, the impact of the fixed foundation is more pronounced in front of the turbine and in the region between the turbines. Many studies have been performed on capturing the hydrodynamic interactions of wave energy farms focusing on the diffraction and radiation effects [5–8]. Perez et al. [9] studied a combined system containing an Oscillating Water Column (OWC) with the monopile substructure of a floating offshore wind turbine, wherein

* Corresponding author.
E-mail address: v.raghavan@tudelft.nl (V. Raghavan).

https://doi.org/10.1016/j.renene.2024.121577
Received 29 April 2024; Received in revised form 19 July 2024; Accepted 9 October 2024
Available online 10 October 2024

a detailed analysis of the incident and reflective waves from the hybrid system and the Response Amplitude Operators (RAOs) for the free surface of the OWC were validated against experimental results.

Borg et al. [10] proposed the idea of using a WEC on a floating platform as a way to reduce the hydrodynamic loads on the FOWT foundations as well as absorb energy through a Power Take-Off (PTO) system simultaneously. By tuning the WEC to have its natural frequency close to that of the FOWT, most energy could be captured by the WEC while maintaining small damping ratios. Furthermore, maximum motion reduction of the FOWT was achieved by having a WEC with a natural frequency slightly below that of the FOWT. Gkaraklova et al. [11] investigated a circular array of semi-immersed heaving WECs around a hybrid wind-wave monopile through a frequency-domain model and reported that the power absorption ability of the array was significantly improved under both regular (≈ 50% increase in peak power absorbed) and irregular waves (≈ 60% increase in peak power absorbed). Gonzalez et al. [12] optimized the control of a collocated offshore wind wave farm, wherein a time-domain hydrodynamic model was developed to evaluate the wave field.

Frequency-based numerical tools and methods have been widely deployed in the field of renewables, because: (a) they can provide accurate and reliable results at the preliminary design stage and (b) their output (frequency-dependent hydrodynamic quantities) are required for their integrated analysis in time-domain. Among those methods, the boundary integral equation method (BIEM) based on the linear potential flow theory is one of the most popular choices. In BIEM, the boundary integral equations are derived from the Green's functions and these can be numerically solved by discretizing the structures into a large number of boundary elements [13]. This method of discretization referred to as panel methods for solving BIEM have been in employed in popular commercial codes such as WAMIT (Wave Analysis MIT) [14] and ANSYS AQWA [15] as well as open-source solvers such as Nemoh [16], Capytaine [17], Aquadyn [18], with WAMIT and Nemoh being the most popular. Both WAMIT and Nemoh have BIEM frameworks, that allow for diffraction radiation computations with multiple bodies. Although Capytaine has been used for the analysis of single structures [19], the hydrodynamic interactions considering multiple bodies have not been validated yet. The same holds true for Aquadyn, which has only been used for analysing single bodies [20]. Therefore, Nemoh is currently the only available open-source option for evaluating hydrodynamic fluid–structure interactions for multiple bodies.

WAMIT implements Newman's polynomial approximation methods for the calculation of the free-surface Green's function, which allows for fast, accurate and reliable computations. On the other hand, Nemoh employs an interpolation method, wherein the wave part of the Green's function is calculated by interpolating the entries from a look-up table, which can require high computational effort depending on the number of coefficients needed. This can range from 64,000 to 2,00,000 entries [21].

HAMS [13,22] is a recently developed open-source BIEM solver which employs approximation methods for the Green's functions similar to Newman's methods. It offers some advantages over popular solvers WAMIT and Nemoh for certain cases. The work of Raghavan et al. [23] showed the high computational speeds of HAMS as compared to both WAMIT (2-3x) and Nemoh (10–20x) for the cases of a semi-immersed cylindrical point buoy as well as a Oscillating Surge Wave Energy Converter (OSWEC), while also providing accurate results very close to that of WAMIT. The work of Sheng et al. [24] showed that HAMS provides better accuracy than Nemoh, as well as better speed of simulations as compared to both WAMIT and Nemoh when no parallelization is implemented. They tested several cases of a semi-immersed cylindrical point buoy, the TALOS WEC, a semi-immersed cylindrical point buoy with a heave plate, semi-immersed cylindrical point buoy, with gaps and semi-immersed cylindrical point buoy with overlapping panels. Furthermore, when creating models with thin structures (such as a heave plate) and overlapping panels (examples include joints of structures, modelling an OWC in a two-body system where the internal water column modelled as a piston overlaps with the hull of the OWC), HAMS matched the accuracy of WAMIT, while Nemoh is unable to deal diffraction-radiation computation when panels there are overlapping panels.

Uzunoglu et al. [25] compared HAMS and WAMIT for the hydrodynamic analysis of the CENTEC-TLP free float design. In the barge mode, it has moon-pool type openings to improve the towing dynamics, which make this a complex geometry. Within the frequency domain, the hydrodynamic coefficients in HAMS and WAMIT delivered almost identical results. Similar results were observed for the RAOs. Furthermore, when extending the study to a time-domain analysis, almost identical response were obtained from the two solvers.

HAMS being an open-source solver, shows considerable potential for marine renewable energies and offshore structures, owing to its high computational efficiency and accuracy compared to other open-source solvers such as Nemoh. One feature it currently lacks is the ability to analyse hydrodynamic interactions considering multiple bodies [13,22, 24]. Immense applications are available within the field of renewables including modelling offshore wind farms, wave farms, hybrid wind-wave, collocated wind-wave farms as well as individual devices such as the OWC that requires specific considerations.

This study extends the single body HAMS to multiple-body formulations and validates its performance with several floating concepts. The multi-body formulations incorporate the approaches used in Newman [26] and Kashiwagi et al. [27], through the evaluation of the diffraction and radiation boundary integral equations. These formulations are utilized to determine the hydrodynamic coefficients and exciting forces for exemplary WECs/multi-column foundations for OWTs represented by cylindrical/spherical geometries, OWCs etc, thus showcasing a wide array of multiple body fluid structure interaction problems that can be resolved by HAMS-MREL. This is done for both shallow and deep water cases. The incorporated formulations are then validated with semi-analytical solutions as well as verified using a cross-model comparison with the commercial BIEM solver WAMIT. Offering a comprehensive validation of the physics, the extended new version is referred to as HAMS-,MREL (Marine Renewable Energies Lab) to signify its distinction from the existing single body formulation.

Another new element for HAMS-MREL is the openMP parallelization, that has been extended and validated for the multiple body interaction problem, hence providing a computationally efficient and highly accurate open source BIEM solver for multi-bodies. The study elaborates on comparisons between HAMS-MREL and WAMIT for the considered cases and key insights into the codes themselves. With this formulation, the authors hope to cover the gap of an open-source highly accurate and computationally efficient BIEM solver with a wide array of applicability.

Section 2 introduces the numerical formulation leading up to the boundary integral equations and then providing the solution strategy for the obtained set of algebraic equations, Section 3 discusses the validation of HAMS-MREL with semi-analytical solutions, and/or cross-model validation with WAMIT for four test cases, Section 4 discusses the comparison between WAMIT and HAMS in terms of the computational resources utilized, Section 5 discusses the potential reasons for differences and similarities between HAMS-MREL and WAMIT focusing on the numerical algorithms implemented in the two codes. Section 6 highlights the main conclusions of this research. Section 7 discusses further developments we are implementing in HAMS-MREL as part of future work.

2. Numerical formulation and solution in HAMS-MREL

This section presents the formulation and solution of the fluid–structure interaction problem within HAMS-MREL. The multiple body

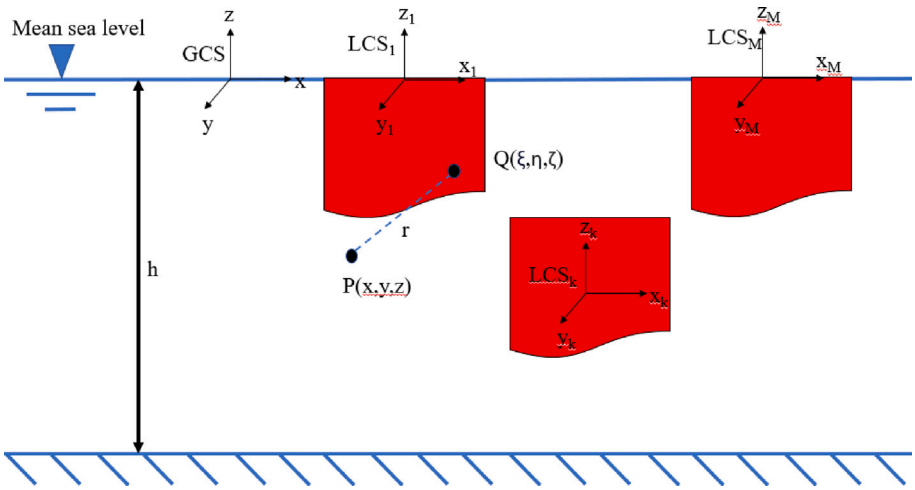

Fig. 1. Definition of the coordinate system for the multiple body interaction problem. *GCS* refers to the global coordinate system and *LCS* refers to the local coordinate system per body. *Q* denotes the source point on the immersed body surface and *P* denotes the field point anywhere in the fluid domain.

fluid-interaction problem is first introduced based on the linear potential flow theory and relevant boundary conditions. These are used to derive the boundary integral equations both in diffraction and radiation. Finally, the derivation of the hydrodynamic coefficients and exciting forces are explained.

2.1. Velocity potential functions

The flow considering multiple bodies with variable geometries within the linear potential flow theory is assumed to be inviscid, irrotational, incompressible and free of flow-separation effects. This is a fluid–structure interaction problem with M bodies (body can be floating or submerged) where the fluid in this case is water (this is shown in Fig. 1). The flow is described through a total complex spatial velocity potential $\phi(x, y, z)$ for all bodies which can be expressed as a combination of three parts: the complex spatial incident wave potential $\phi_I(x, y, z)$, the complex spatial scattered potential $\phi_S(x, y, z)$ and the complex spatial radiated potential $\phi_R(x, y, z)$. (x, y, z) refers to the Cartesian coordinates expressed in m.This is shown in the following equation:

$$\phi = \phi_I + \phi_S + \phi_R = \phi_D + \phi_R \tag{1}$$

The potential satisfies the Laplace equation given as:

$$\nabla^2\phi = 0 \tag{2}$$

In Eq. (1), ϕ_D is the complex spatial diffraction potential. The considered potentials are used for both finite and infinite depth conditions.

To obtain the hydrodynamic coefficients and exciting forces, the diffraction and radiation potentials need to be computed by solving the diffraction and radiation boundary integral equation problem respectively. The boundary conditions for these problems as well as the boundary integral equations are explained the following sub-sections.

2.2. Diffraction problem

The formulation of the diffraction problem for a single floating body within HAMS is provided in the work of Liu [22]. The single body diffraction problem can be extended to incorporate interaction due to the presence of M bodies by building upon the single body fluid interaction.

The boundary conditions to be satisfied by the total diffraction potential, are on the free surface (Eq. (3)), on the body surface (Eq. (4)), at the sea bottom (Eq. (5)), and in the far field (Eq. (6) shows Sommerfield's radiation condition). The boundary conditions are shown as follows.

$$\frac{\partial\phi_D}{\partial z} = \mu\phi_D, z = 0 \tag{3}$$

where $\mu = \omega^2/g$ is the deepwater wave number and g is the acceleration due to gravity.

$$\frac{\partial\phi_D}{\partial n} = 0, \text{on } S_B^{(k)} \tag{4}$$

where $S_B^{(k)}$ is the body surface of the kth body. This boundary condition applies to all bodies.

$$\frac{\partial\phi_D}{\partial z} = 0, z = -h, \text{or } z \to \infty \text{ depending on the depth condition} \tag{5}$$

$$\lim_{R\to\infty}[\sqrt{\mu R}(\frac{\partial\phi_D}{\partial R} - i\mu\phi_D)] = 0 \tag{6}$$

where h denotes the water depth considering finite depth, R is the horizontal distance from any of the bodies and $'i'$ refers to the imaginary unit with its coefficient referring to the imaginary part of a complex number. Within this formulation, the Sommerfield's radiation condition should be satisfied at large distances from the group of bodies.

To derive the boundary integral equations for the diffraction problem with the Green's function approach as an extension of the fluid-body interaction with HAMS, mixed source/dipole boundary integral equations are derived. The scattered potential for body k, $k = 1, \ldots, M$, should consider the contribution from all bodies including itself. The boundary integral equation considering this with $S_B^T = S_B^{(1)} + S_B^{(2)} + \cdots + S_B^{(M)}$ can then be given as follows:

$$2\pi\phi_S(x) + \iint_{S_B^T}\phi_S(\xi)\left(\frac{\partial G(\xi;x)}{\partial n_\xi}\right)dS_\xi = -\iint_{S_B^T}\left(\frac{\partial\phi_I}{\partial n}\right)G(\xi;x)dS_\xi \tag{7}$$

Here x refers to the field point, ξ refers to the source point, G is the Green's function and the subscript $'I'$ indicating the incident wave. The Green's function for the shallow and deep water conditions are explained in detail in the work of Liu [22] and Liang et al. [28] respectively. The velocity potential for the incident wave can be specified based on the complex wave amplitude and the wave frequency. In deep water, the velocity potential of the incoming plane harmonic wave can be defined as:

$$\phi_I = -\frac{igA}{\omega}e^{\mu z}e^{i\mu(x\cos\beta + y\sin\beta)} \tag{8}$$

and for shallow depth as:

$$\phi_I = -\frac{igA}{\omega}\frac{\cosh\nu(z+h)}{\cosh\nu h}e^{ik(x\cos\beta + y\sin\beta)} \tag{9}$$

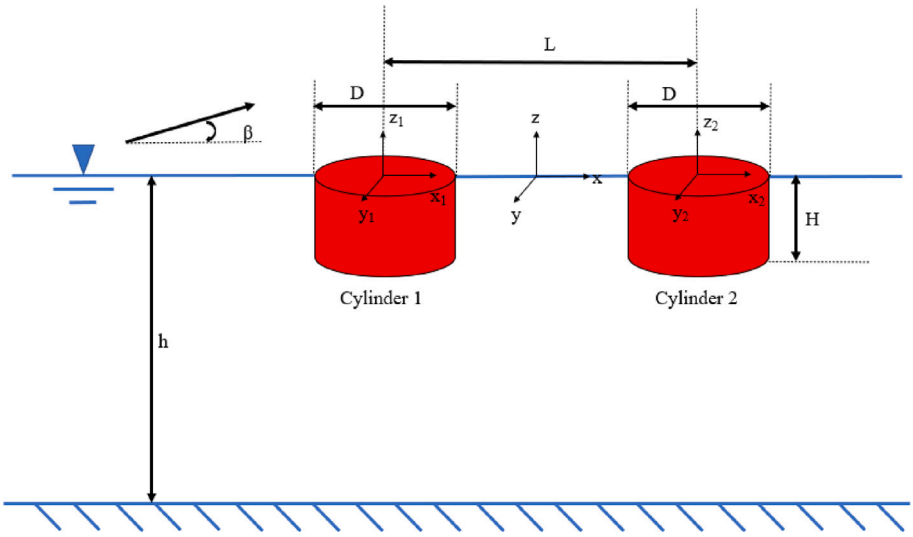

Fig. 2. Two semi-immersed cylinders (Case 1).

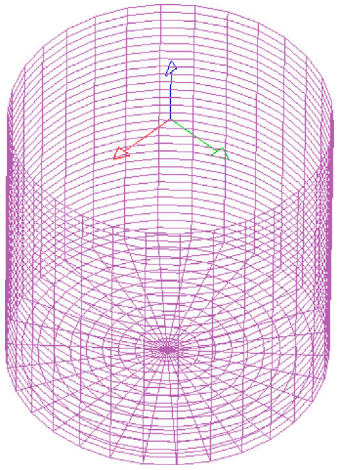

Fig. 3. Cylindrical mesh with 1200 panels used in Case 1.

where β is the angle between the direction of propagation of the incident wave and the positive x-axis, and ν is the wavenumber, defined as the real positive root of the respective water wave dispersion equation.

2.3. Radiation problem

The radiation problem can be extended in a similar way to that of the diffraction problem. It is assumed that the considered body is in motion with all the remaining bodies being stationary. This is obtained from the body surface boundary condition. Together with this boundary condition, all the boundary conditions are given (Eq. (10)–Eq. (13)).

$$\frac{\partial \phi_j^{(k)}}{\partial z} = \mu \phi_j^{(k)}, z = 0 \tag{10}$$

$$\frac{\partial \phi_j^{(k)}}{\partial n} = n_j^{(k)}, \text{on } S_B^{(k)} \tag{11}$$

Here $\phi_j^{(k)}$ refers to the radiation potential of the fluid velocity field generated by the jth degree of freedom (dof) for the kth body. $j = 1, \ldots, 6$ and $k = 1, \ldots, M$. $n_j^{(k)}$ is the normal vector in the jth dof for the kth body. As stated previously, when the kth body is in motion, all the other bodies are assumed to be stationary.

$$\frac{\partial \phi_j^{(k)}}{\partial z} = 0, z = -h, \text{or } z \to \infty \text{ depending on the depth condition} \tag{12}$$

$$\lim_{R\to\infty} [\sqrt{\mu R}(\frac{\partial \phi_j^{(k)}}{\partial R} - i\mu \phi_j^{(k)})] = 0 \tag{13}$$

Similar to the diffraction problem, the boundary integral equation for the complete radiation problem can be given as follows:

$$2\pi \phi_j^{(k)}(x) + \iint_{S_B^T} \phi_j^{(k)}(\xi) \left(\frac{\partial G(\xi; x)}{\partial n_\xi} \right) dS_\xi = \iint_{S_B^T} G(\xi; x) \frac{\partial \phi_j^{(k)}}{\partial n} dS_\xi \tag{14}$$

Considering the boundary condition on the body surface (Eq. (11)), this can be reduced to the following equation:

$$2\pi \phi_j^{(k)}(x) + \iint_{S_B^T} \phi_j^{(k)}(\xi) \left(\frac{\partial G(\xi; x)}{\partial n_\xi} \right) dS_\xi = \iint_{S_B^{(k)}} G(\xi; x) n_j^{(k)} dS_\xi \tag{15}$$

2.4. Discretization of the Integral Equations and solution of the linear algebraic system

The boundary surfaces are discretized into a set of quadrilateral or triangular plane panels to approximate the exact geometry of the bodies. The radiation and diffraction velocity potentials are represented by piecewise constant functions over each panel, as in the existing HAMS formulation [22]. By extending the existing 'collection' method wherein the centroids of the panels represent the collection points, the boundary integral equation for the diffraction problem (Eq. (7)) is discretized into:

$$2\pi \phi_S(x_i) + \sum_{l=1}^{N_p^T} D_{il} \phi_S(x_l) = \sum_{l=1}^{N_p^T} S_{il} V_I(x_l), (i = 1, 2, \ldots, N_p^T) \tag{16}$$

Here N_p^T is the summation of panels over all bodies. The integrations of the sources and dipoles within the mixed source/dipole formulation over each panel for the scattering problem is given as follows:

$$D_{il} = \iint_{S_{B,l}} \frac{\partial G(\xi; x_i)}{\partial n_\xi} dS_\xi \tag{17}$$

$$S_{il} = \iint_{S_{B,l}} G(\xi; x_i) dS_\xi \tag{18}$$

and

$$V_I(x_l) = -\frac{\partial \phi_I}{\partial n}(x_l) \tag{19}$$

Similarly, the collection method can be applied to the radiation problem and is given as:

$$2\pi \phi_j^{(k)}(x_i) + \sum_{l=1}^{N_p^T} D_{il} \phi_j^{(k)}(x_l) = \sum_{m=1}^{N_p^k} S_{im} n_j^{(k)}(x_m) \tag{20}$$

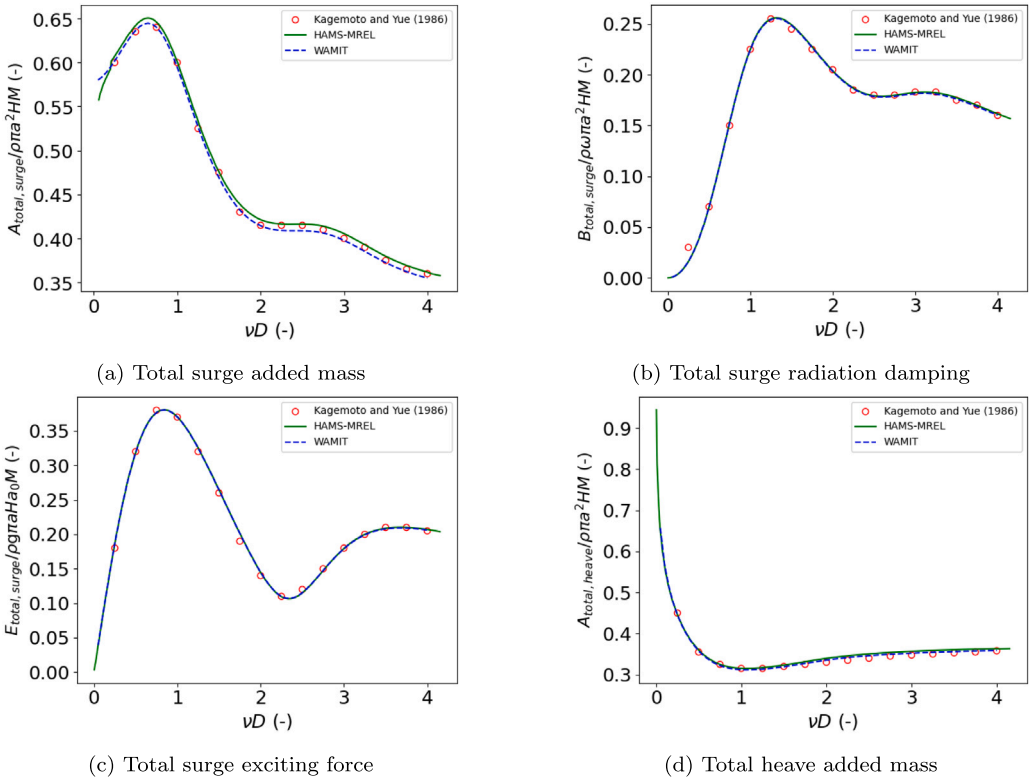

(a) Total surge added mass

(b) Total surge radiation damping

(c) Total surge exciting force

(d) Total heave added mass

Fig. 4. Hydrodynamic coefficients and exciting forces for both cylinders in Case 1.

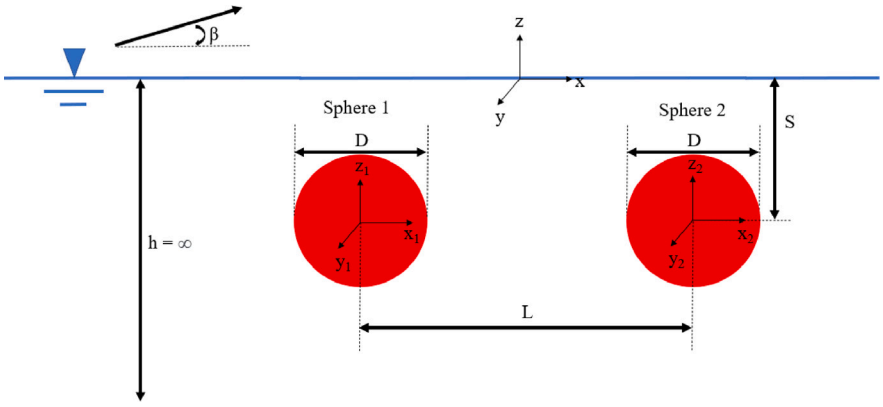

Fig. 5. Two submerged sphere interaction problem (Case 2).

with $i = 1, 2, \ldots, N_p^{(M)}$, $j = 1, 2, \ldots, 6$ and

$$n_j^{(k)}(x_l) = \frac{\partial \phi_j^{(k)}}{\partial n}(x_l) \tag{21}$$

This assembly for the radiation problem is done for all M bodies to obtain the final set of linear algebraic equations for all M bodies.

For both the diffraction and radiation problem, N_p^T number of linear equations are obtained which need to be solved simultaneously. The LU decomposition solver currently available in the HAMS package is adapted to solve the set of linear algebraic equations for both the diffraction and radiation problem.

2.5. Derivation of the hydrodynamic coefficients and exciting forces

Once the velocity potentials on the body surfaces are obtained, the hydrodynamic coefficients and exciting forces can be computed based on [27]. By integrating the pressure multiplied by the jth component of the normal vector over the kth body, the hydrodynamic forces acting in the jth dof of the kth body can be computed. These is as follows:

$$E_j^{(k)} = i\omega\rho \iint_{S_B^k} \phi_D n_j^{(k)} dS \tag{22}$$

$$A_{js}^{(k)(q)} - iB_{js}^{(k)(q)} = \rho \iint_{S_B^k} \phi_j^{(q)} n_s^{(k)} dS \tag{23}$$

where $E_j^{(k)}$ is the wave exciting force in the jth dof of the kth body, and $A_{js}^{(k)(q)}$ and $B_{js}^{(k)(q)}$ are the added mass and radiation damping coefficients, respectively, in the sth dof of the kth body due to the jth mode of motion of the qth body.

2.6. OpenMP parallelization on machines with multiple cores

Within the existing HAMS formulation, OpenMP, an application programming interface (API) for writing shared memory parallel applications had been implemented. Being easily implementable for existing

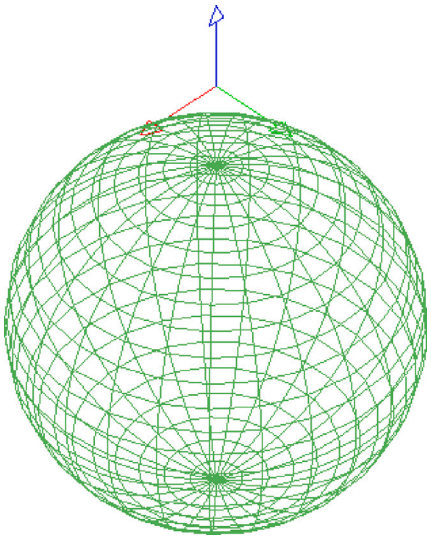

Fig. 6. Spherical mesh with 625 panels used in Case 2.

serial codes and highly suitable for multi-core architectures, it was chosen to adapt its current implementation for the multi-body formulation as well. This was done for the computation of the Green's function, resolving the complex linear system of algebraic equations as well as the calculation of the hydrodynamic coefficients and exciting forces.

3. Validation of HAMS-MREL

This section focuses on the validation of HAMS-MREL. Various geometrical shapes in finite and infinite depth condition are showcased focusing on the field of renewables while considering the availability of analytical/semi-analytical solutions of other investigators found in literature. These include cylindrical/spherical shapes, that are used for point absorber WECs, multi-column foundations for offshore wind turbines, submerged pressure differential WEC and OWCs. Validation is realized through comparison of hydrodynamic coefficients and exciting forces with those obtained from analytical/semi-analytical solutions and/or from WAMIT. For all the cases, with regard to the HAMS meshes, the normal vector of the panels points from the body towards the fluid.

3.1. Case 1 - Semi-immersed cylinders

The solutions for the hydrodynamic coefficients and exciting forces from interaction theory proposed by Kagemoto and Yue in [29] for a two semi-immersed floating cylinder were used for validation here.

The theory considers plane wave diffraction and radiation within the formulation of the linear potential flow for multiple bodies. The propagating and evanescent wave fields (also referred to as local waves) are decomposed into cylindrical waves in terms of Henkel and modified Bessel functions. To account for the interactions among the bodies when solving the diffraction problem, the scattered potential ϕ_i^S for the ith body is represented through the incident potentials ϕ_j^I of body j, $j \neq i$ based on addition theorems for Bessel functions. Furthermore, the authors use the diffraction characteristics of an isolated body through "diffraction transfer matrices" that relate to the incident and diffracted cylindrical partial waves. The derivation of the radiation problem follow closely with the development here (see [30] and [31]). The radiation coefficients are derived from the culmination of radiation coefficients of a body in isolation in combination with the partial cylindrical wave contributions (both propagating and evanescent) from the scattering and incident potentials. In addition to the aforementioned algebraic method, a cross-model comparison is also carried out here with WAMIT.

Table 1
Properties used for the simulation in HAMS-MREL and WAMIT for Case 1.

Property	Unit	Value
Diameter, D	m	4
Spacing, L	m	5.2
Water Depth, h	m	8
Draft, H	m	4
Angle of incidence, β	deg	0

The two-cylinder case is shown in Fig. 2, 1200 panels were used for the mesh (shown in Fig. 3) for both WAMIT and HAMS-MREL in this comparison. The properties selected for the two-cylinder case have been shown in Table 1. The number of panels were based on a convergence study that was carried out, and the mesh discretization is exactly the same in HAMS-MREL and WAMIT to minimize discrepancies. Fig. 4(a) shows the total surge added mass (Eq. (24)), Fig. 4(b) shows the total surge radiation damping (Eq. (25)), Fig. 4(c) shows the total surge exciting forces (Eq. (26)) and Fig. 4(d) shows the total heave added mass (Eq. (27)) for the two cylinders together. The quantities are made dimensionless as indicated in the figures. , $D = 2a$ with a is the radius of the cylinder and a_0 is the wave amplitude. Refer to Eq. (22) and Eq. (23) for the definitions of the exciting force and hydrodynamic coefficients respectively.

$$A_{total,surge} = A_{11}^{(1)(1)} + A_{11}^{(1)(2)} + A_{11}^{(2)(1)} + A_{11}^{(2)(2)} \tag{24}$$

$$B_{total,surge} = B_{11}^{(1)(1)} + B_{11}^{(1)(2)} + B_{11}^{(2)(1)} + B_{11}^{(2)(2)} \tag{25}$$

$$E_{total,surge} = |E_1^{(1)} + E_1^{(2)}| \tag{26}$$

$$A_{total,heave} = A_{33}^{(1)(1)} + A_{33}^{(1)(2)} + A_{33}^{(2)(1)} + A_{33}^{(2)(2)} \tag{27}$$

As seen from the results, HAMS-MREL is close to both WAMIT as well as the semi-analytical method. For the total surge added mass, HAMS-MREL slightly under-predicts the results as compared to the algebraic solution, particularly for $\nu D > 2$. However, it can also be seen that WAMIT slightly over-predicts the values as compared to the semi-analytical solution in the same regime. The potential reasons for these differences between HAMS-MREL and WAMIT are mentioned in Section 5.

3.2. Case 2 - Two submerged spheres

The semi-analytical solution for two interacting submerged spheres is used for validation from the work of Wu [32]. This case was chosen to highlight the capability of HAMS-MREL for modelling submerged bodies, as this would be crucial to model devices such as the submerged pressure differential WEC among others. A spherical geometry is chosen to showcase a different geometry as compared to Case 1.

Wu's work extends on the multipole expansion theory proposed by Thorne [33] for a single sphere using the linear potential flow theory. The theory proposed by Thorne expresses the velocity potential through a series of singularities placed within the considered body. With the extension of this theory, Wu proposes an interaction theory that is applicable for any number of spheres with arbitrary radii and submerges.

The two submerged sphere case is shown in Fig. 5. The properties considered are shown in Table 2. The mesh used within HAMS-MREL and WAMIT is shown in Fig. 6. The semi-analytical solution for the hydrodynamic coefficients and exciting forces from Wu [32] were compared with HAMS-MREL and WAMIT for the cases of surge (Fig. 7), sway (Fig. 8) and heave Fig. 9. All the results are for the Sphere 2.

In all cases, it can be observed that the results from HAMS-MREL exactly match to both the semi-analytical solution from Wu [32] as well as WAMIT.

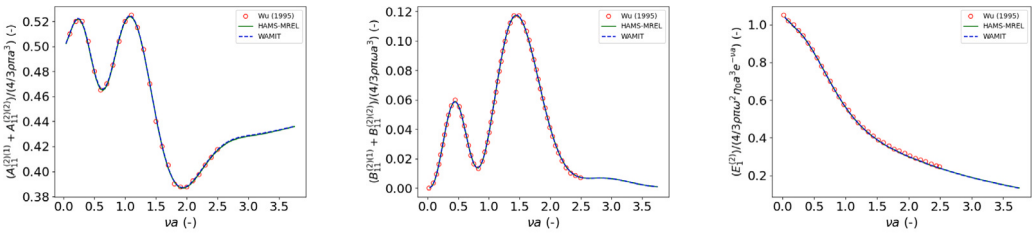

(a) Surge added mass (b) Surge radiation damping (c) Surge exciting force

Fig. 7. Hydrodynamic coefficients and exciting forces for surge of Sphere 2.

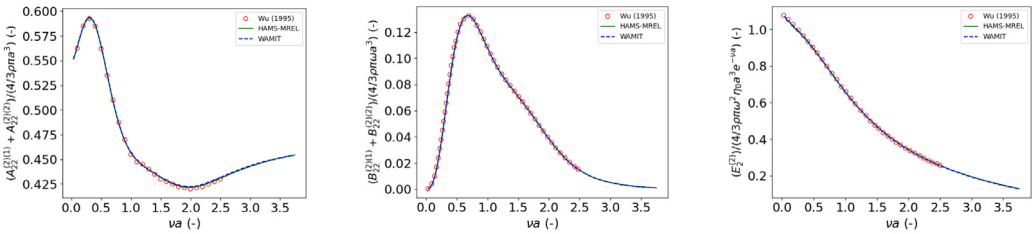

(a) Sway added mass (b) Sway radiation damping (c) Sway exciting force

Fig. 8. Hydrodynamic coefficients and exciting forces for sway of Sphere 2.

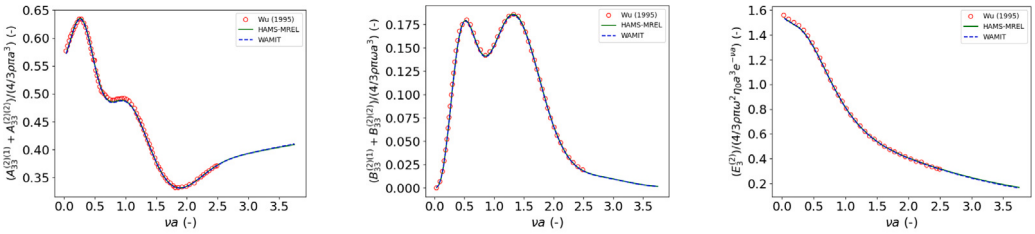

(a) Heave added mass (b) Heave radiation damping (c) Heave exciting force

Fig. 9. Hydrodynamic coefficients and exciting forces for heave of Sphere 2.

Table 2
Properties used for the simulation in HAMS-MREL and WAMIT for Case 2.

Property	Unit	Value
Diameter, D	m	6
Spacing, $L = 4a$	m	12
Water Depth, h	m	Infinite
Submergence, S	m	9
Angle of incidence, β	degrees	45

3.3. Case 3 - Three semi-submerged cylinders

The third case for validation is taken from the work by Mavrakos [34], which provides a solution for the hydrodynamic coefficients based on a semi-analytical method. The work focuses on obtaining the hydrodynamic coefficients (added mass and radiation damping) from the different combination of axisymmetric bodies. Here the cylindrical case is considered. This case was chosen as it allows for validation of hydrodynamic coefficients for pitching motion as well as solving a fluid-body interaction problem with greater than two bodies, which is observed in all the other cases.

The radiation problem is solved using an semi-analytical method that combines single body hydrodynamic characteristics with the multiple scattering approach to account for the interaction phenomena. By superimposing various orders of radiated/scattered waves emanating from one body oscillating in the vicinity of the others, the velocity potential is derived for each body within the multi-component system. This methodology is applicable for any number of axisymmetric bodies with any geometrical arrangement, provided the vertical projections of any two bodies not overlap.

The three semi-immersed floating cylinder problem is shown in Fig. 10. The mesh used for this case in both HAMS-MREL and WAMIT is shown in Fig. 11. The properties selected for the three-cylinder case have been shown in Table 3. The number of panels were based on a convergence study that was carried out as part of the research.

The results comparing the added mass in surge and pitch-surge for cylinder 1 is shown in Figs. 12(a) and 12(b). HAMS-MREL is very close to the semi-analytical solution and WAMIT for $va < 1.5$. Beyond that, small differences are observed between HAMS-MREL and WAMIT. The results comparing the radiation damping in surge and pitch-surge for cylinder 1 is shown in Figs. 12(c) and 12(d) respectively. The results for the surge added mass and radiation damping for cylinder 2 are plotted in Fig. 13(a) and Fig. 13(b) respectively. A trend similar to cylinder 1 is observed. The potential reasons for these differences are explained in Section 5.

3.4. Case 4 - Floating OWC

The final validation case selected is that of a floating OWC. In addition to modelling a new type of wave energy device with an internal water column, as compared to the first three cases, this case also highlights the capability of HAMS-MREL in delivering accurate solutions when the source and field points are very close.

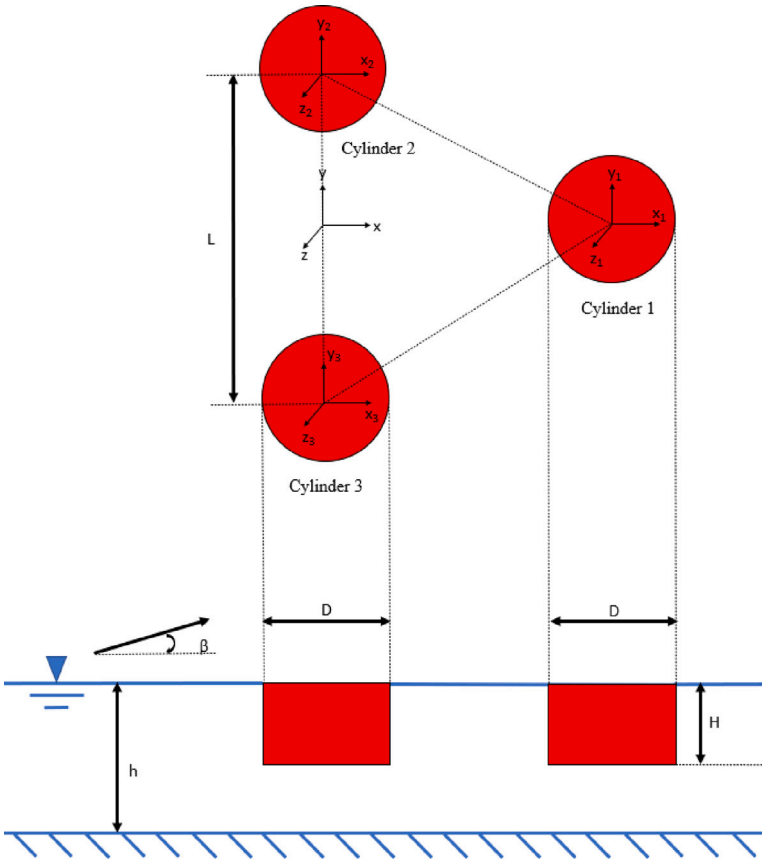

Fig. 10. Three semi-immersed floating cylinders (Case 3).

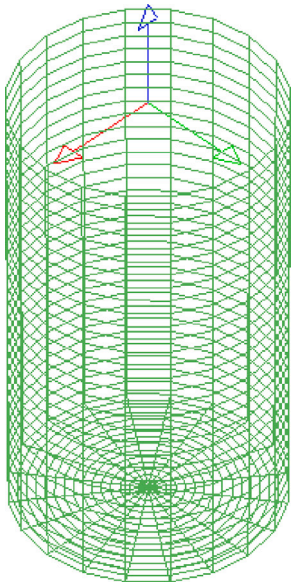

Fig. 11. Cylindrical mesh with 900 panels used in Case 3.

Table 3
Properties used for the simulation in HAMS-MREL and WAMIT for Case 3.

Property	Unit	Value
Radius, b	m	6
Spacing, l	m	15
Water Depth, d	m	120
Draft, H	m	10.95
Angle of incidence, β	degrees	0

Most literature showing modelling approaches for OWCs with BIEM utilize WAMIT as the BIEM solver, particularly when doing experimental validations. To this extent, WAMIT is also the most developed BIEM solver for OWCs as it offers the ability to model the OWC in two different ways. The first method models an imaginary piston above the internal water column as a thin massless disk in combination with generalized degrees of freedom that can use all 6 modes [35] (usually heave is only used). This method utilizes dipole panels to model the thin disk, which also requires a high resolution for the mesh. However, since only the disk is modelled with dipole panels, the computational effort is reasonable. The second method models the hull of the OWC and an imaginary piston in a two-body system, where the length of the piston is varied so as to replace part of the water column [36]. This is particularly useful when the water column moves only in heave.

The second method is adopted here for modelling the floating OWC in HAMS-MREL since it does not have the feature of generalized degrees of freedom for modelling the massless disk. An inter-model comparison is performed with WAMIT. The case from the work of Penalba et al. [37] has been considered wherein a simplified version of the Sparbuoy is modelled. The length of the imaginary piston is chosen to be equal to the length of the column based on the work of Sheng et al. [36] since this better captures the hydrodynamics of the OWC system including the added mass at infinite frequency, which becomes essential when performing time domain analysis of the OWC system.

It has been shown in the work of Sheng [36], that considering different lengths of the piston will result in different added masses due in heaving. However, the total mass, which is equal to the sum of the mass of the piston (which is the mass of the water column replaced by the piston from the free surface to the length of the water column)

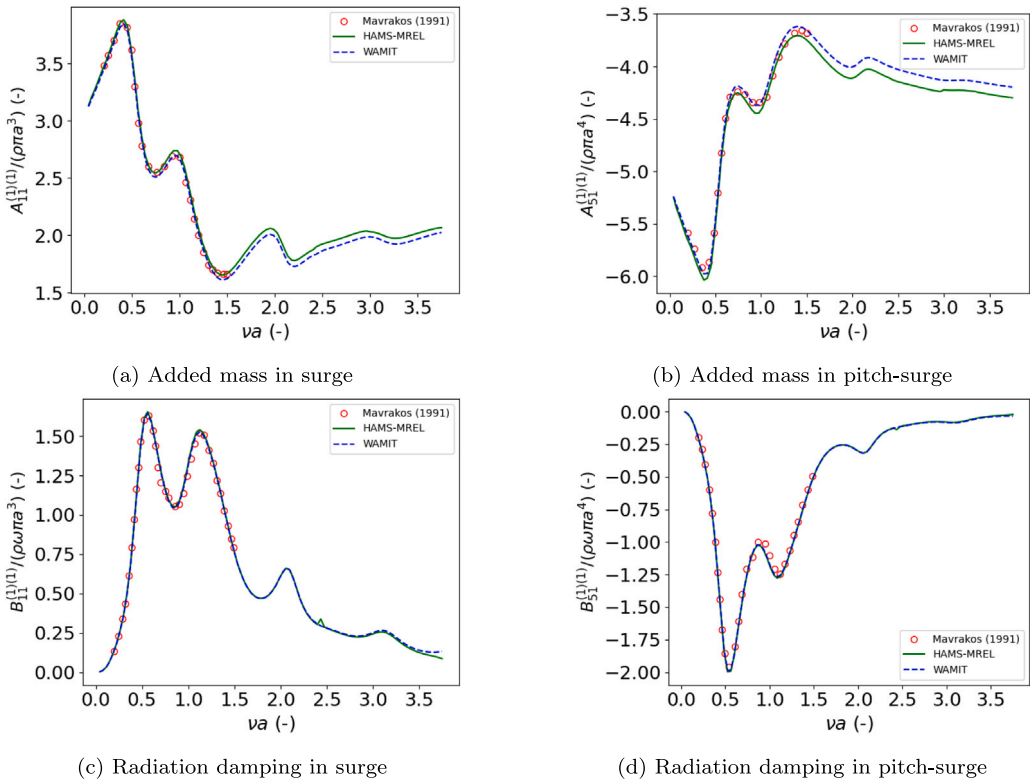

(a) Added mass in surge

(b) Added mass in pitch-surge

(c) Radiation damping in surge

(d) Radiation damping in pitch-surge

Fig. 12. Hydrodynamic coefficients for surge and pitch-surge for Cylinder 1.

Table 4
Properties used for the simulation in HAMS-MREL and WAMIT for Case 4.

Property	Unit	Value
Inner Radius, r_1	m	2
Outer Radius, r_2	m	3
Water Depth, h	m	Infinite
Draft, H	m	10
Angle of incidence, β	degrees	0

Table 5
Simulation times for the 4 cases with HAMS-MREL and WAMIT (Time in min).

Case	N_p^T	N_ω	WAMIT	HAMS-MREL
Case 1	2400	80	18.00	131.50
Case 1 Infinite depth	2400	80	9.25	9.30
Case 2	1250	100	6.00	3.05
Case 3	2700	100	65.45	716.67
Case 3 Infinite depth	2700	100	61.86	23.67
Case 4 two body system	1024	202	18.5	4.16

and the added mass due to the heaving piston, are approximately constant over all considered piston lengths. Therefore, the combination of added mass and mass of the piston in HAMS-MREL, as obtained from the second method, is compared here with the added mass obtained with the generalized modes case (first method) and two-body method (second method) as obtained from WAMIT. These comparisons are shown assuming motion only in heaving.

The meshes for the two considered cases are shown in Figs. 15 and 16. When modelling the OWC with the generalized modes, the internal column surface mesh is modelled as part of the hull mesh. The properties of the model are specified in Table 4. The number of panels used for the two-body case was based on a convergence study conducted as part of this research. The results for the total mass (added mass + mass of piston) is shown in Fig. 17 and the radiation damping is shown in Fig. 18. As seen, the results match perfectly between the two codes validating this extension of HAMS-MREL for obtaining a solution with overlapping panels.

4. Computational resources

This section focuses on comparing the computation time between WAMIT and HAMS-MREL for the four cases considered. Furthermore, the parallelization capabilities of HAMS-MREL for multiple bodies are investigated with varying number of cores.

Comparison is done between WAMIT and HAMS-MREL in terms of the analysis time for the considered four cases. In addition to the four mentioned cases, two for finite depth (Case 1 and Case 3) and two for infinite depth (Case 2 and Case 4), two additional cases are considered. Specifically, Case 1 and Case 3 are also analysed in infinite depth to compare the analysis time between finite and infinite depth cases. The analyses were carried out in a 4 core, 8 GB RAM PC with a Intel Core i5-4440 CPU processor (3.10 GHz). The computation times for the analyses are shown in Table 5. Since WAMIT v6.1 was used for these analyses, no parallelization was available in WAMIT. Accordingly, for this comparison, no parallelization was used in HAMS-MREL.

In Table 5, N_p^T is the total number of panels and N_ω is the number of frequencies used in the analysis. From Table 5, it can be observed that for the considered infinite depth cases, HAMS-MREL is generally 2 to 4 times faster than WAMIT, whereas for the considered finite depth cases, it is 7 to 11 times slower than WAMIT. HAMS-MREL does employ parallelization, which can speed up the calculations. This feature was added in WAMIT for v7 or higher [24].

To explore parallelization in HAMS-MREL, the analyses were carried on the Snellius High Performance Computer (SURF Netherlands) for Cases 1 and 3, both for finite and infinite depth conditions. All the analyses were carried out in a 64 GB node with AMD Rome 7H12 processor (3.3 GHz). The number of cores for the calculations were varied from 1 core to 32 cores. The computation ratio (Percentage ratio

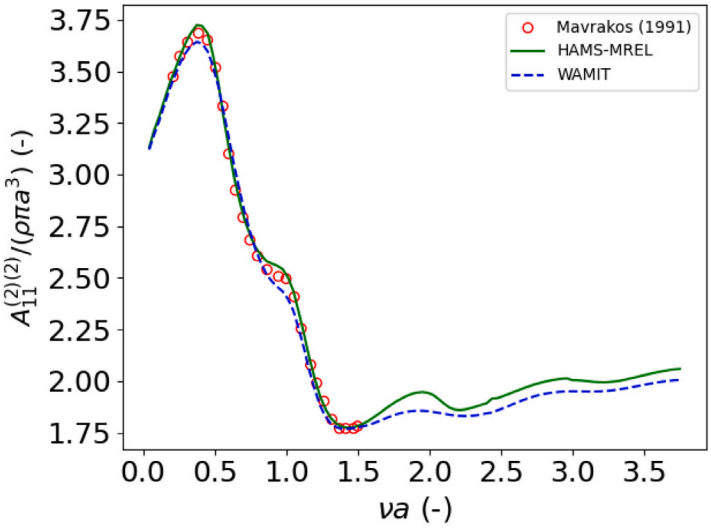

(a) Added mass in surge

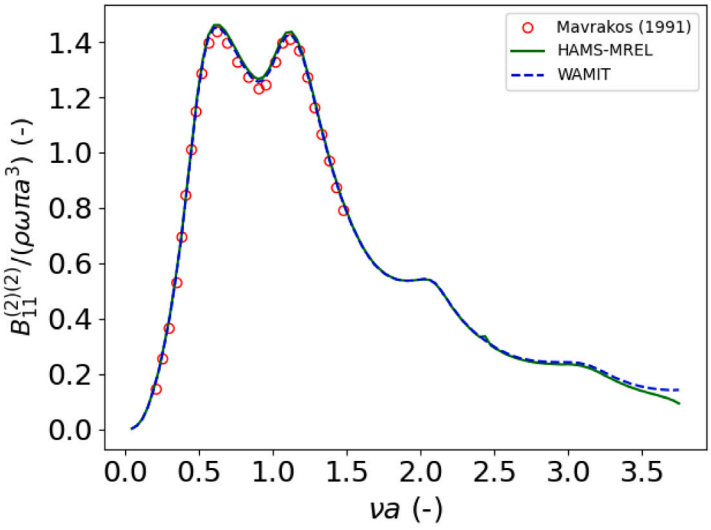

(b) Radiation damping in surge

Fig. 13. Hydrodynamic coefficients for surge cylinder 2.

of the speed in p cores to the speed with one core, where p varies from 1 to 32) with the number of cores is shown in Fig. 19 and the speed-up ratio (ratio of the speed in 1 core to the speed with n core, where n varies from 1 to 32) with the number of cores is shown in Fig. 20. As seen, the computations can be speeded up as much as 12 to 14 times for the finite depth cases as compared to the infinite depth case, where the ratio is a little over 2.

This also shows the effectiveness of the OpenMP parallelization in HAMS-MREL with regard to the finite depth cases, where it also takes the most time. Comparing the finite depth and infinite depth cases, the finite depth cases are 5 to 3 times slower than the infinite depth cases with increasing number of cores.

5. Discussion

Case 1 and Case 3 have the finite depth condition, while Case 2 and Case 4 have the infinite depth condition. For the infinite depth cases, the results from WAMIT and HAMS-MREL are very close to each other. When solving for the infinite depth free-surface Green's function, WAMIT breaks down the entire flow domain into four sub-domains based on parameters $X = \nu R$ and $Y = \nu|z+h|$ (R is the distance between the source and field point and h is the water depth). Different semi-analytical expansions are used to approximate the Green's function in each sub-domain as proposed by Newman [21]. In HAMS, a different approach is used with a global approximation algorithm utilized which is valid within the entire flow region, that is used to compute the infinite depth Green's function which is accurate up to the second order, as proposed by Liang et al. [28]. Liang et al. mentions that Newman's algorithms, as well as the proposed global approximation algorithms within HAMS-MREL have an accuracy of up to 10^{-6}. This could explain why HAMS-MREL and WAMIT are very close for the infinite depth cases.

When considering Cases 1 and Case 3, which have the finite depth condition, some differences are observed. These are observed at $\nu a > 1.5$ particularly for the added mass in surge and pitch-surge degrees of freedom and slightly for the radiation damping for the same degrees of freedom for Case 3. There could be two potential reasons for this:

1. The algorithms used for the computations of the finite depth Green's functions: Similar to WAMIT, HAMS (and HAMS-MREL) decomposes the flow domain into four sub-domains based on the ratio R/h to evaluate the finite depth free-surface Green's

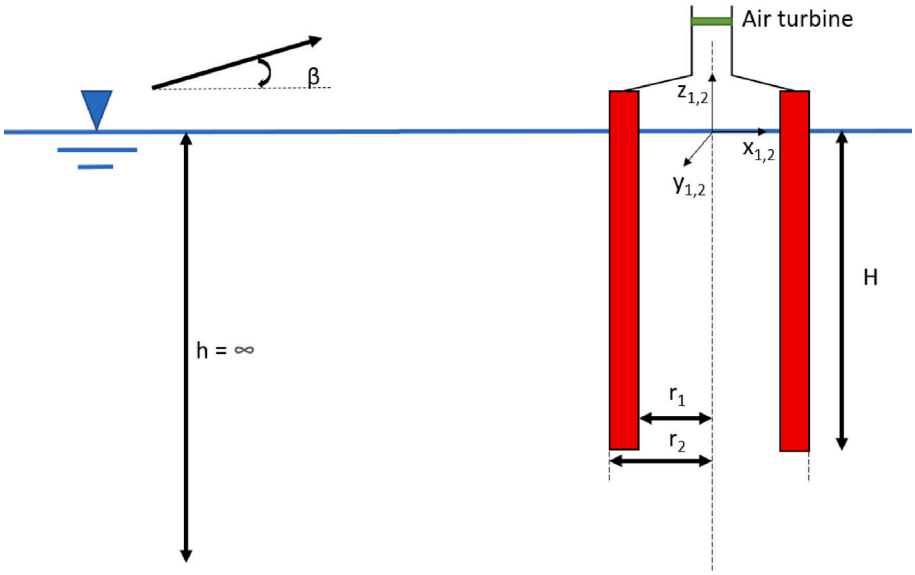

Fig. 14. Floating OWC (Case 4).

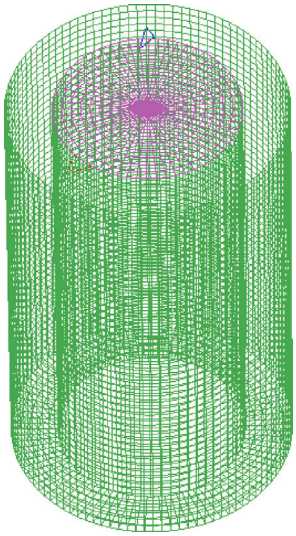

Fig. 15. Modelling Sparbuoy floating OWC using a thin massless disk for the piston in combination with generalized mode in heave. Thin disk (purple) and hull of OWC (green). 2275 panels in total across the entire model.

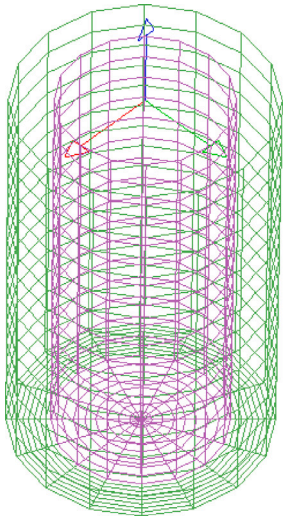

Fig. 16. Modelling Sparbuoy floating OWC as a two-body system where the piston is modelled to the length of the internal water column. Internal water surface (purple) and hull of OWC (green). 640 panels for the hull and 384 panels for the internal water column.

function; Here R is the distance between the source point and the target point, and h is the water depth. HAMS (and HAMS-MREL) employs different semi-analytical expansions in different regimes including one in the vicinity of the logarithmic singularity [13]. To make the algorithm computationally efficient, expressions are derived to calculate the number of terms for these semi-analytical solutions, which are based on performing meticulous convergence studies [13]. In WAMIT, the polynomial expansions in different domains are computed based on evaluating the converging solution of the Green's function, as part of the algorithm itself.

2. The solver used for solving the set of linear algebraic equations: WAMIT offers three different solvers (i) A special iterative solver, (ii) a direct solver, and a (iii) block iterative solver. For the considered finite depth cases, the special iterative solver was utilized, based on generalized minimum residual, that obtains the lowest residual error. This solver is highly recommended for lower order panels (in this we work with the constant panel method), and does not require temporary storage which makes it computationally efficient [38]. For both case 1 and 3, convergence was obtained with a maximum of 22 iterations. In HAMS-MREL, a direct solver based on LU decomposition is the only currently available option. This was incorporated in the original HAMS tool as it only requires the left side of the matrix (for both the diffraction and radiation problem) to be evaluated once even for multiple wave headings, making the solver computationally efficient when calculating the hydrodynamic coefficients and exciting forces in a variety of sea states and incident wave angles [13]. The usage of two different solvers between HAMS-MREL and WAMIT could also be contributing to the differences observed the results of Case 1 and 3.

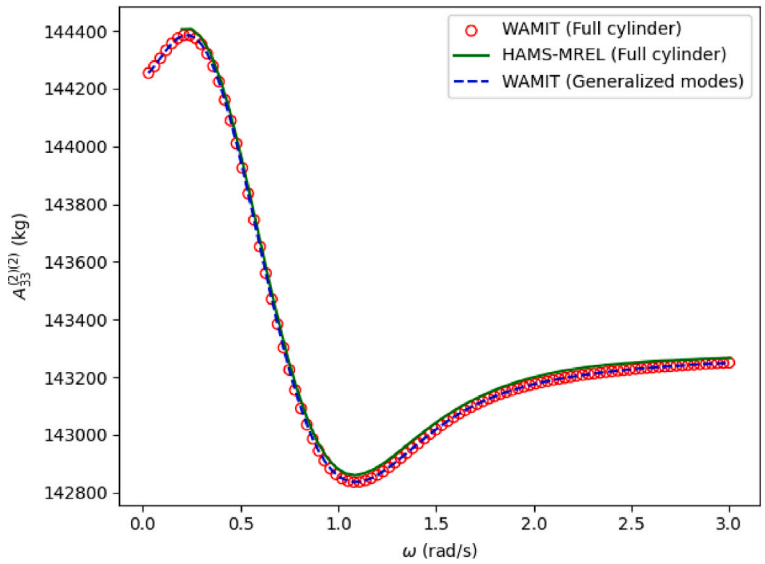

Fig. 17. Total mass (Mass of piston + Added mass) in heaving for the internal free surface.

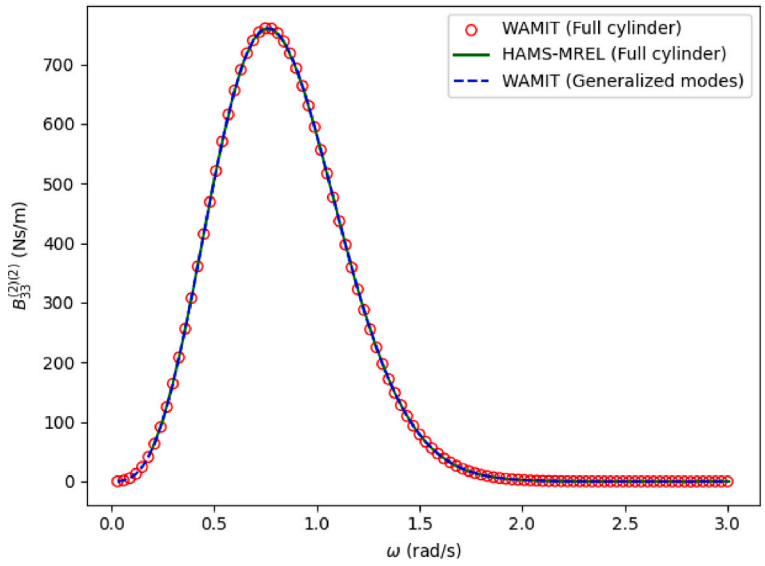

Fig. 18. Radiation damping in heaving for the internal free surface.

Comparing the differences in computational resources between finite and infinite depth cases for the two solvers, it is observed that HAMS-MREL is generally faster than WAMIT for the considered infinite depth cases, while WAMIT is faster than HAMS-MREL for the considered finite depth cases. The parts of the code that are expected to take the most time is the computation of the Green's function [13], followed by the solution to the set of linear algebraic equations. While the computational time of the iterative solver in WAMIT is proportional to $(N_p^T)^2$, the computation time for the direct solver with LU decomposition in HAMS-MREL is proportional to $(N_p^T)^3$ [39]. Therefore, for the infinite depth cases it is possible that the calculation of the Green's function in HAMS-MREL compensates for the lower speed of its direct solver, thus making it faster than WAMIT. However, in the finite depth cases, the increased computation time due to the direct solver in HAMS-MREL is not compensated by the computation of the finite depth Green's function. This is hard to confirm in WAMIT, since it is commercial and its code is not accessible. It should be noted, that all comparisons are drawn when the same number of panels are considered in both HAMS-MREL and WAMIT. WAMIT offers the possibility of symmetry, which could significantly make it faster. However, this is not within the scope of this research, since the focus is on comparing HAMS-MREL with its current capabilities as an open-source solver.

6. Conclusions

The paper presents a new open-source multiple body solver HAMS-MREL, which can be considered as an extension for the existing fast, reliable and robust solver HAMS. Building upon the multiple body interaction theory provided by Newman and Kashiwagi, the diffraction and radiation boundary integral equations are derived and solved to obtain the hydrodynamic coefficients and exciting forces for all bodies. This is done for both finite and infinite depth cases.

To validate the proposed formulation, the hydrodynamic coefficients and exciting forces obtained from HAMS-MREL are compared with semi-analytical solutions found in literature along with inter-model comparison with the popular and widely used commercial BIEM solver WAMIT (v6.1) for four cases. The cases are selected based on varying geometries being representative of various floating structures within the field of renewable energy including point absorbers,

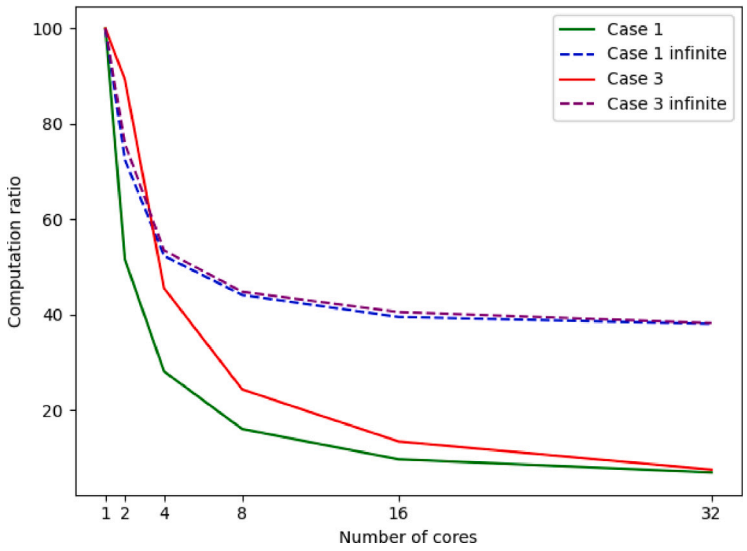

Fig. 19. Computation ratio with number of cores for Case 1 and 3 - Finite and Infinite depth.

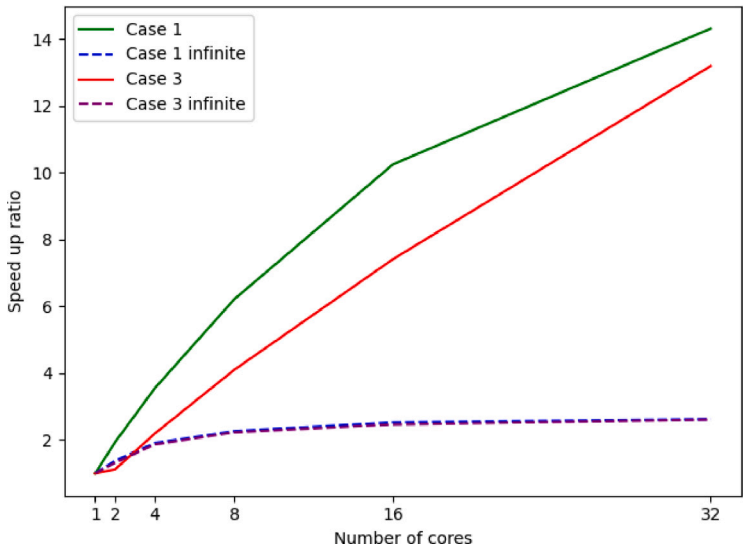

Fig. 20. Speed up ratio with number of core for Case 1 and 3 - Finite and Infinite depth.

submerged pressure differential WECs, multi-column foundations for offshore wind turbines and OWCs.

When considering the finite depth cases, it is generally observed that HAMS-MREL is close to the semi-analytical solutions as well as the commercial solver WAMIT with minor differences. The potential reasons for these differences could be the difference in the algorithms used to solve the finite depth Green's functions as well as the solver used to solve the set of linear algebraic equations. When considering the infinite depth cases, HAMS-MREL matches perfectly with both the semi-analytical solutions as well as the commercial solver WAMIT.

Considering the computation times between HAMS-MREL and WAMIT, it is observed that for the considered deep water cases, HAMS-MREL is generally 2 to 4 times faster than WAMIT. For the considered finite depth cases, HAMS-MREL is 7 to 11 times slower. This is potentially due to the balance between the time taken for solving the set of linear algebraic equations (direct solver in HAMS-MREL vs iterative solver in WAMIT) and the computation of infinite/finite depth Green's functions. All comparisons are drawn when the same number of panels are considered in both HAMS-MREL and WAMIT. WAMIT offers the possibility of symmetry, which could significantly make it faster. This is however not within the scope of this research since the focus is on comparing HAMS-MREL with its current capabilities as an open-source solver. Within the HAMS-MREL formulation, OpenMP parallelization has also been implemented as part of this work. Therefore considering parallelization, the computations can be speeded up to 12 to 14 times for the finite depth cases, and up to 2 times for infinite depth cases, when comparing single core to 32 core computations, which shows its computational effectiveness.

While there are many commercial BIEM solver with multiple body interactions (WAMIT, ANSYS AQWA, WADAM), there is a lack of highly accurate, computationally efficient and parallelized validated open-source BIEM solvers. With this research, the authors hope to contribute to the open-source domain; and enable the development of highly accurate and highly efficient numerical tools, for the deployment of marine renewable energies, such as wave energy arrays and floating wind.

7. Future work

The authors are currently working on adding more features to HAMS-MREL, as well as improving on existing features. The new features in the pipeline include removal of irregular frequencies, global

symmetry, generalized modes and wave fields (free surface displacement and pressure) considering multi-body interaction. Furthermore, the authors are also looking into the implementation of more computationally efficient solvers such as the iterative solvers based on generalized least residuals method as well as mesh refinement techniques for more complicated geometries.

CRediT authorship contribution statement

Vaibhav Raghavan: Writing – review & editing, Writing – original draft, Validation, Software, Methodology, Investigation, Formal analysis, Data curation, Conceptualization. **Eva Loukogeorgaki:** Writing – review & editing, Writing – original draft, Validation, Supervision, Methodology, Investigation, Conceptualization. **Nikos Mantadakis:** Writing – review & editing, Validation, Software, Investigation. **Andrei V. Metrikine:** Writing – review & editing, Supervision, Resources, Methodology, Conceptualization. **George Lavidas:** Writing – review & editing, Writing – original draft, Supervision, Resources, Project administration, Methodology, Investigation, Funding acquisition, Conceptualization.

Declaration of competing interest

The authors declare the following financial interests/personal relationships which may be considered as potential competing interests: Vaibhav Raghavan reports financial support was provided by European Commission.

Acknowledgements

The authors would like to thank Yingyi Liu, the creator of HAMS for the initial discussions regarding the original code. Without his original robust code, this implementation would not have been possible.

This research has received funding from the European Union's Horizon 2020 research and innovation programme under grant agreement No. 101006927 (VALID). The authors would also like to thank the WECANet COST Action 17105 Short Term Scientific Mission (STSM), Greece, for providing an extended travel research grant for wave energy arrays, that gave us ideas for further development. The authors would also like to acknowledge SURF and access to the HPC Snellius for running the simulations in HAMS-MREL, under project EINF3290.

References

[1] UN nations - global issues - population, 2022, URL https://www.un.org/en/global-issues/population. (Accessed 28 May 2023).

[2] EU Strategy for Offshore Renewables, 2020, URL https://energy.ec.europa.eu/topics/renewable-energy/offshore-renewable-energy_en#:~:text=The%20strategy%20sets%20targets%20for,GW%2C%20respectively%2C%20by%202050. (Accessed 10 July 2023).

[3] C. Pérez-Collazo, D. Greaves, G. Iglesias, A review of combined wave and offshore wind energy, Renew. Sustain. Energy Rev. (ISSN: 1364-0321) 42 (2015) 141–153, http://dx.doi.org/10.1016/j.rser.2014.09.032, URL https://www.sciencedirect.com/science/article/pii/S1364032114008053.

[4] Giorgia Sismani, Aurélien Babarit, Eva Loukogeorgaki, Impact of fixed bottom offshore wind farms on the surrounding wave field, in: ISOPE, in: Proc. of the International Symposium on Offshore and Polar Engineering (ISOPE2016), Rhodes, Greece, 2016, http://dx.doi.org/10.17736/ijope.2017.ts11, URL https://hal.science/hal-01492657.

[5] François Charrayre, Christophe Peyrard, Michel Benoit, Aurélien Babarit, A Coupled Methodology for Wave-Body Interactions at the Scale of a Farm of Wave Energy Converters Including Irregular Bathymetry, in: International Conference on Offshore Mechanics and Arctic Engineering, Volume 8A: Ocean Engineering, 2014, http://dx.doi.org/10.1115/OMAE2014-23457, V08AT06A043.

[6] L.M. de la Torre-Castro, R.C.R. Pascal, Y. Perignon, A. Babarit, G.S. Payne, Combined impact of power take-off capping and of wave resource description on wave energy converter performance, Appl. Ocean Res. (ISSN: 0141-1187) 134 (2023) 103494, http://dx.doi.org/10.1016/j.apor.2023.103494, URL https://www.sciencedirect.com/science/article/pii/S014111872300038X.

[7] Grgur Tokić, Dick K.P. Yue, Axisymmetric reflectors in wave energy converter arrays: Harnessing scattering to increase energy extraction, Phys. Fluids (ISSN: 1070-6631) 35 (6) (2023) 067120, http://dx.doi.org/10.1063/5.0155209.

[8] Yao Liu, Norimi Mizutani, Yong-Hwan Cho, Tomoaki Nakamura, Nonlinear hydrodynamic analysis and optimization of oscillating wave surge converters under irregular waves, Ocean Eng. (ISSN: 0029-8018) 250 (2022) 110888, http://dx.doi.org/10.1016/j.oceaneng.2022.110888, URL https://www.sciencedirect.com/science/article/pii/S0029801822003250.

[9] C. Perez-Collazo, D. Greaves, G. Iglesias, Hydrodynamic response of the WEC sub-system of a novel hybrid wind-wave energy converter, Energy Convers. Manage. (ISSN: 0196-8904) 171 (2018) 307–325, http://dx.doi.org/10.1016/j.enconman.2018.05.090, URL https://www.sciencedirect.com/science/article/pii/S0196890418305740.

[10] Michael Borg, Maurizio Collu, Feargal P. Brennan, Use of a wave energy converter as a motion suppression device for floating wind turbines, Energy Procedia (ISSN: 1876-6102) 35 (2013) 223–233, http://dx.doi.org/10.1016/j.egypro.2013.07.175, URL https://www.sciencedirect.com/science/article/pii/S1876610213012617.

[11] Sofia Gkaraklova, Pavlos Chotzoglou, Eva Loukogeorgaki, Frequency-based performance analysis of an array of wave energy converters around a hybrid wind–wave monopile support structure, J. Mar. Sci. Eng. (ISSN: 2077-1312) 9 (1) (2021) http://dx.doi.org/10.3390/jmse9010002, URL https://www.mdpi.com/2077-1312/9/1/2.

[12] Hector Del Pozo Gonzalez, Fernando D. Bianchi, Jose Luis Dominguez-Garcia, Oriol Gomis-Bellmunt, Co-located wind-wave farms: Optimal control and grid integration, Energy (ISSN: 0360-5442) 272 (2023) 127176, http://dx.doi.org/10.1016/j.energy.2023.127176, URL https://www.sciencedirect.com/science/article/pii/S0360544223005704.

[13] Yingyi Liu, Shigeo Yoshida, Changhong Hu, Makoto Sueyoshi, Liang Sun, Junliang Gao, Peiwen Cong, Guanghua He, A reliable open-source package for performance evaluation of floating renewable energy systems in coastal and offshore regions, Energy Convers. Manage. (ISSN: 0196-8904) 174 (2018) 516–536, http://dx.doi.org/10.1016/j.enconman.2018.08.012, URL https://www.sciencedirect.com/science/article/pii/S0196890418308562.

[14] C.-H. Lee, J.N. Newman, X. Zhu, An Extended Boundary Integral Equation Method for the Removal of Irregular Frequency Effects, Internat. J. Numer. Methods Fluids 23 (7) (1996) 637–660, http://dx.doi.org/10.1002/(SICI)1097-0363(19961015)23:7<637::AID-FLD437>3.3.CO;2-V, URL https://ui.adsabs.harvard.edu/abs/1996IJNMF..23..637L.

[15] ANSYS. Ansys AQWA v14.5 2012, 2012, URL https://www.ansys.com/products/structures/ansys-mechanical. (Accessed 28 May 2023).

[16] Aurélien Babarit, Gérard Delhommeau, Theoretical and numerical aspects of the open source BEM solver NEMOH, in: 11th European Wave and Tidal Energy Conference, EWTEC2015, in: Proceedings of the 11th European Wave and Tidal Energy Conference, Nantes, France, 2015, URL https://hal.science/hal-01198800.

[17] Matthieu Ancellin, Frédéric Dias, Capytaine: a Python-based linear potential flow solver, J. Open Source Softw. 4 (36) (2019) 1341, http://dx.doi.org/10.21105/joss.01341.

[18] Gérard Delhommeau, Seakeeping Codes AQUADYN and AQUAPLUS, in: Proceedings of the 19th WEGEMT SCHOOL on Numerical Simulation of Hydrodynamics: Ships and Offshore Structures, Nantes, France, 1993.

[19] Matthieu Ancellin, Marlène Dong, Philippe Jean, Frédéric Dias, Far-field maximal power absorption of a bulging cylindrical wave energy converter, Energies (ISSN: 1996-1073) 13 (20) (2020) http://dx.doi.org/10.3390/en13205499, URL https://www.mdpi.com/1996-1073/13/20/5499.

[20] João M.B.P. Cruz, António J.N.A. Sarmento, Sea state characterisation of the test site of an offshore wave energy plant, Ocean Eng. (ISSN: 0029-8018) 34 (5) (2007) 763–775, http://dx.doi.org/10.1016/j.oceaneng.2006.04.004, URL https://www.sciencedirect.com/science/article/pii/S0029801806001545.

[21] John Nicholas Newman, Algorithms for the free-surface green function, J. Engrg. Math. (ISSN: 1573-2703) 19 (1985) 57–67, http://dx.doi.org/10.1007/BF00055041, URL https://link.springer.com/article/10.1007/BF00055041#article-info.

[22] Yingyi Liu, HAMS: A frequency-domain preprocessor for wave-structure interactions—Theory, development, and application, J. Mar. Sci. Eng. (ISSN: 2077-1312) 7 (3) (2019) http://dx.doi.org/10.3390/jmse7030081, URL https://www.mdpi.com/2077-1312/7/3/81.

[23] V. Raghavan, G. Lavidas, A.V. Metrikine, N. Mantadakis, E. Loukogeorgaki, A comparative study on BEM solvers for wave energy converters, CRC Press, London, 2022, pp. 441–447, http://dx.doi.org/10.1201/9781003360773-50, URL https://www.taylorfrancis.com/books/9781003360773/chapters/10.1201/9781003360773-50,

[24] W. Sheng, E. Tapoglou, X. Ma, C.J. Taylor, R.M. Dorrell, D.R. Parsons, G. Aggidis, Hydrodynamic studies of floating structures: Comparison of wave-structure interaction modelling, Ocean Eng. (ISSN: 0029-8018) 249 (2022) http://dx.doi.org/10.1016/j.oceaneng.2022.110878, URL https://www.sciencedirect.com/science/article/pii/S0029801822003183.

[25] Ebru Uzunoglu, Yingyi Liu, Carlos Guedes Soares, Performance of the open-source potential flow solver HAMS in estimating the hydrodynamic properties of a floating wind turbine, CRC Press, London, 2022, pp. 619–627, http://dx.doi.org/10.1201/9781003360773-70, URL https://www.taylorfrancis.com/chapters/edit/10.1201/9781003360773-70,

[26] John Nicholas Newman, Wave Effects on Multiple Bodies, 2001.

[27] Meshashi Kashiwagi, Kazuaki Endo, Hiroshi Yamaguchi, Wave drift forces and moments on two ships arranged side by side in waves, Ocean Eng. (ISSN: 0029-8018) 32 (5) (2005) 529–555, http://dx.doi.org/10.1016/j.oceaneng.2004.09.005, URL https://www.sciencedirect.com/science/article/pii/S0029801804002252.

[28] Hui Liang, Huiyu Wu, Francis Noblesse, Validation of a global approximation for wave diffraction-radiation in deep water, Appl. Ocean Res. (ISSN: 0141-1187) 74 (2018) 80–86, http://dx.doi.org/10.1016/j.apor.2018.02.025, URL https://www.sciencedirect.com/science/article/pii/S0141118718300075.

[29] Hiroshi Kagemoto, Dick K.P. Yue, Interactions among multiple three-dimensional bodies in water waves: an exact algebraic method, J. Fluid Mech. 166 (1986) 189–209, http://dx.doi.org/10.1017/S0022112086000101.

[30] F. Fàbregas Flavià, C. McNatt, F. Rongère, A. Babarit, A.H. Clément, A numerical tool for the frequency domain simulation of large arrays of identical floating bodies in waves, Ocean Eng. (ISSN: 0029-8018) 148 (2018) 299–311, http://dx.doi.org/10.1016/j.oceaneng.2017.11.026, URL https://www.sciencedirect.com/science/article/pii/S0029801817306935.

[31] Yingyi Liu, Hui Liang, Masashi Kashiwagi, Peiwen Cong, Alternative approaches of evaluating diffraction transfer matrix and radiation characteristics using the hybrid source-dipole formulation, Appl. Ocean Res. (ISSN: 0141-1187) 114 (2021) 102769, http://dx.doi.org/10.1016/j.apor.2021.102769, URL https://www.sciencedirect.com/science/article/pii/S0141118721002455.

[32] G.X. Wu, The interaction of water waves with a group of submerged spheres, Appl. Ocean Res. (ISSN: 0141-1187) 17 (3) (1995) 165–184, http://dx.doi.org/10.1016/0141-1187(95)00010-0, URL https://www.sciencedirect.com/science/article/pii/0141118795000100.

[33] R.C. Thorne, Multipole expansions in the theory of surface waves, Math. Proc. Cambridge Philos. Soc. 49 (4) (1953) 707–716, http://dx.doi.org/10.1017/S0305004100028905.

[34] S.A. Mavrakos, Hydrodynamic coefficients for groups of interacting vertical axisymmetric bodies, Ocean Eng. (ISSN: 0029-8018) 18 (5) (1991) 485–515, http://dx.doi.org/10.1016/0029-8018(91)90027-N, URL https://www.sciencedirect.com/science/article/pii/002980189190027N.

[35] M. Rosati, J.C.C. Henriques, J.V. Ringwood, Oscillating-water-column wave energy converters: A critical review of numerical modelling and control, Energy Convers. Manage. X (ISSN: 2590-1745) 16 (2022) 100322, http://dx.doi.org/10.1016/j.ecmx.2022.100322, URL https://www.sciencedirect.com/science/article/pii/S2590174522001453.

[36] Wanan Sheng, Raymond Alcorn, Anthony Lewis, Assessment of primary energy conversions of oscillating water columns. I. Hydrodynamic analysis, J. Renew. Sustain. Energy (ISSN: 1941-7012) 6 (5) (2014) http://dx.doi.org/10.1063/1.4896850, 053113.

[37] Markel Penalba, Thomas Kelly, John Ringwood, Using NEMOH for modelling wave energy converters: A comparative study with WAMIT, in: 12th European Wave and Tidal Energy Conference, EWTEC, 2017, URL https://mural.maynoothuniversity.ie/12466/.

[38] Chang Ho Lee, John Nicholas Newman, WAMIT user manual, versions 6.4, 6.4pc, 6.3s, 6.3s-PC, 2015-11-6.

[39] Xuewei Ping, Hongjie Wang, Qingbo Li, Xinghui Yin, Xinjun Wang, Changli li, A discussion on the solution of linear systems appeared in gradient coil optimization with the finite element method, Appl. Magn. Reson. 51 (2020) http://dx.doi.org/10.1007/s00723-020-01189-y.